Langmuir Article

pubs.acs.org/Langmuir

Bimetallic Flowers, Beads, and Buds: Synthesis, Characterization, and Raman Imaging of Unique Mesostructures

P. R. Sajanlal and T. Pradeep*

DST Unit on Nanoscience (DST UNS), Department of Chemistry and Sophisticated Analytical Instrument Facility, Indian Institute of Technology Madras, Chennai - 600 036, India

Received June 9, 2009. Revised Manuscript Received September 7, 2009

We demonstrate the creation of a new class of nano/mesostructures, such as Au/Ag flowers, Au/Pt buds, and Au/Pt beads, through the directed overgrowth of Ag or Pt on Au/oligoaniline nanowires (Au/OA NWs). Different stages of the formation of these mesostructures have been studied using various spectroscopic and microscopic techniques. The surface plasmon resonance (SPR) of the Au/OA NWs can be tuned by the incorporation of bimetallicity into the nanowire. Raman based spectral imaging of the bimetallic Au/Ag mesoflower and Au/Pt mesobud revealed the molecular details and the nature of interaction of oligoaniline with the different metal domains. Raman study also suggested a substrate effect due to the different domains of the mesostructures, and spectral images distinguished these two regions. The single particle spectral images suggest that the material is surface-enhanced Raman active.

Introduction

Recent research in nanochemistry focuses on the development of various synthetic pathways to produce nanoparticles of diverse shapes and composition in order to tailor their chemical and physical properties. Bimetallic nanoparticles belong to an important class of nanomaterials, since they exhibit multifunctional properties due to the effective coupling of different metal domains.[1] Core−shell[2] nanoparticles and bimetallic nanorods[3] are two interesting classes of materials made with noble metals. Unusual bimetallic nanoparticles such as nanorice,[4] nanocorns,[5] nanoboxes,[6] nanocobes,[7] triangular nanoframes,[8] and nano dumbbells[9] are also reported. Hybrid nanostructures such as Pt/Au nanowires[10] and Au/Pd tadpole-like[11] nanostructures have been synthesized by simple galvanic displacement reaction. These hybrid nanostructures find applications in diverse areas such as biosensing,[12] catalysis,[13] electronics,[14] and electro-optic nanodevices. It has been reported that the optical and catalytic properties[15] of hybrid nanomaterials of gold and platinum can be tuned within a single nanostructure. Pt nanoparticles can also be used as nucleation agents for the synthesis of magnetic nanoparticles.[16] The presence of metal tips or surfaces on such materials allows the anchoring of organic molecules or biomolecules and hence can be used in the sensing of various targets of interest.[17]

Complex anisotropic nanostructures are desirable from the point of view of near-infrared absorption[18] and surface-enhanced Raman spectroscopy (SERS).[19] Among these, the latter is a powerful tool to investigate the chemical structure, reactivity, and physical properties of various materials. Extremely weak Raman signals have been proven to be enhanced by the presence of nanoparticles due to enhancements in the scattering cross section. This technique is capable of probing the chemical heterogeneity of the materials at high spatial resolution. A Raman based image can provide adequate contrast without using any staining agents and can be utilized for biological imaging. To explore the fascinating shape and composition dependent properties, it is necessary to develop a simple method for the shape-controlled synthesis of such novel bimetallic nanoparticles. The synthesis of bimetallic nanostructures without hard templates[20] is attractive because of the controllability and easiness in making nanoparticles of diverse shapes.

In this report, we present the synthesis of beautiful nano/mesostructures[21] such as flowers, beads, and buds, made of gold,

*Corresponding author. E-mail: pradeep@iitm.ac.in

(1) Hurst, S. J.; Payne, E. K.; Qin, L.; Mirkin, C. A. *Angew. Chem., Int. Ed.* **2006**, *45*, 2672. (b) Taleb, M.; Rothenberg, E.; Popov, I.; Costi, R.; Banin, U. *Science* **2004**, *304*, 1787.
(2) (a) Xue, C.; Millstone, J. E.; Li, S.; Mirkin, C. *Angew. Chem., Int. Ed.* **2007**, *46*, 8436. (b) Sanedrin, R. G.; Georganopoulou, D. G.; Park, S.; Mirkin, C. A. *Adv. Mater.* **2005**, *17*, 1027.
(3) (a) Song, J. H.; Kim, F.; Kim, D.; Yang, P. *Chem.—Eur. J.* **2005**, *11*, 910. (b) Hunyadi, S. E.; Murphy, C. J. *J. Mater. Chem.* **2006**, *16*, 3929.
(4) Talley, C. E.; Jackson, J. B.; Oubre, C.; Grady, N. K.; Hollars, C. W.; Lane, S. M.; Huser, T. R.; Nordlander, P.; Halas, N. J. *Nano Lett.* **2005**, *5*, 1569.
(5) Teranishi, T.; Inoue, Y.; Nakaya, M.; Oumi, Y.; Sano, T. *J. Am. Chem. Soc.* **2004**, *126*, 9914.
(6) (a) Sun, Y.; Mayers, B.; Xia, Y. *Nano Lett.* **2002**, *2*, 481. (b) Sun, Y.; Xia, Y. *J. Am. Chem. Soc.* **2004**, *126*, 3892.
(7) Gunawidjaja, R.; Peleshanko, S.; Ko, H.; Tsukruk, V. V. *Adv. Mater.* **2008**, *20*, 1544.
(8) Metraux, G. S.; Cao, Y. C.; Jin, R.; Mirkin, C. A. *Nano Lett.* **2003**, *3*, 519.
(9) Huang, C.; Yang, Z.; Chang, H. *Langmuir* **2004**, *20*, 6089.
(10) Teng, X.; Han, W.; Wang, Q.; Li, L.; Frenkel, A. I.; Yang, J. C. *J. Phys. Chem. C* **2008**, *112*, 14697.
(11) Camargo, P. H. C.; Xiong, Y.; Ji, L.; Zuo, J. M.; Xia, Y. *J. Am. Chem. Soc.* **2007**, *129*, 15452.
(12) Nicewarner-PeSa, S. R.; Freeman, R. G.; Reiss, B. D.; He, L.; PeSa, D. J.; Walton, I. D.; Cromer, R.; Keating, C. D.; Natan, M. J. *Science* **2001**, *294*, 137.
(13) (a) Liu, F.; Lee, J. Y.; Zhou, W. *Adv. Funct. Mater.* **2005**, *15*, 1459. (b) Kline, T. R.; Paxton, T. E.; Mallouk, W. F.; Sen, A. *Angew. Chem., Int. Ed.* **2005**, *44*, 744.
(14) (a) Hangarter, C. M.; Myung, N. V. *Chem. Mater.* **2005**, *17*, 1320. (b) Liu, S.; Tok, J. B.-H.; Bao, Z. *Nano Lett.* **2005**, *5*, 1071.
(15) (a) Ah, C. S.; Kim, S. J.; Jang, D.-J. *J. Phys. Chem. B* **2006**, *110*, 5486. (b) Schrinner, M.; Proch, S.; Mei, Y.; Kempe, R.; Miyajima, N.; Ballauff, M. *Adv. Mater.* **2008**, *20*, 1928.
(16) Farrell, D.; Majetich, S.; Wilcoxon, J. *J. Phys. Chem. B* **2003**, *107*, 11022.
(17) Pearce, M. E.; Melanko, J. B.; Salem, A. K. *Pharm. Res.* **2007**, *24*, 2335.
(18) (a) Sajanlal, P. R.; Pradeep, T. *Adv. Mater.* **2008**, *20*, 980. (b) Shankar, S. S.; Rai, A.; Ankamwar, B.; Singh, A.; Ahmad, A.; Sastry, M. *Nat. Mater.* **2004**, *3*, 482. (c) Pas-Blanco, I.; Hoppe, C. E.; Pineiro-Redondo, Y.; López-Quintela, M. A.; Rivas, J. *Langmuir* **2008**, *24*, 983.
(19) (a) Kneipp, K.; Kneipp, H.; Itzkan, I.; Dasari, R. R.; Feld, M. S. *Chem. Rev.* **1999**, *99*, 2957. (b) Campion, A.; Kambhampati, P. *Chem. Soc. Rev.* **1998**, *27*, 241. (c) Wang, H.; Levin, C. S.; Halas, N. J. *J. Am. Chem. Soc.* **2005**, *127*, 14992.
(20) (a) Hulteen, J. C.; Martin, C. R. *J. Mater. Chem.* **1997**, *7*, 1075. (b) Sioss, J. A.; Keating, C. D. *Nano Lett.* **2005**, *5*, 1779.
(21) (a) Xiao, Z.-L.; Han, C. Y.; Kwok, W.-K.; Wang, H.-H.; Welp, U.; Wang, J.; Crabtree, G. W. *J. Am. Chem. Soc.* **2004**, *126*, 2316. (b) Penner, R. M. *J. Phys. Chem. B* **2002**, *106*, 3339. (c) Sajanlal, P. R.; Pradeep, T. *Nano Res.* **2009**, *2*, 306.

silver, and platinum, through a directed overgrowth of Ag or Pt on gold nanowires. The precursor nanowire used throughout the synthesis was a new variety of material made of gold/oligoaniline composite. The surface plasmon resonance (SPR) of the Au nanowire could be tuned by the variation of the composition. The unusual morphology of the precursor gold/oligoaniline nanowire (Au/OA NW) composite plays a key role in the selective overgrowth. The overgrowth of silver and platinum, although extended to cover the gold wire surface completely, can be stopped at appropriate conditions to preserve specific mesostructures. Elemental maps of the nucleation and growth process have been captured showing the systematic evolution of the mesostructures. This method is an example of in situ growth of a three-dimensional (3D) object on a one-dimensional (1D) nanostructure.

The overgrowth of Ag and Pt is attributed to the selective growth of exposed nucleation sites present in Au/OA NWs. A surface-enhanced Raman spectroscopy based imaging of the bimetallic Au/Ag mesoflower and Au/Pt mesobud was performed. We studied the interaction of the oligoaniline coating at different metal domains (gold, silver, and platinum) in detail. The controllability in the selective overgrowth is the main attraction of this work. The synthesis of such an unusual and beautiful 3D nanoscale object shows an example of controlling the composition, dimension, and morphology of materials at a single particle level. In view of the specific size regime in which these structures are formed, we call them mesoflowers (MFs), which implies a specific size range of 10 nm to micrometers, although the structures can be tuned from the nanometer to micrometer range.

Experimental Section

Materials. Tetrachloroauric acid trihydrate ($HAuCl_4 \cdot 3H_2O$), citric acid, ascorbic acid, and $AgNO_3$ were purchased from CDH, India. Aniline and hexachloroplatinic acid ($H_2PtCl_6 \cdot 6H_2O$) were purchased from Sigma Aldrich. All chemicals were used as such without further purification. Triply distilled water was used throughout the experiments.

Synthesis of Au/OA NWs. In a typical synthesis, the solution containing 25 mg of citric acid in 35 mL of water was kept at 80 °C and 1.5 mL of 25 mM $HAuCl_4$ was added. When the color of the solution changed from pale yellow to pink, 100 μL of distilled aniline was added. Heating was continued for 5 more minutes. This solution was kept at room temperature for 3 h and centrifuged at 4000 rpm, and then the black residue was collected. The residue was washed with water two times. The washed black product, containing oligoaniline capped gold NWs, was used for further reaction. The Au/OA NWs were characterized and were suspended in 100 mL of water. This was the starting material for the synthesis of bimetallic flowers. The Au/OA NW suspension was very stable for several months, and no change was found even after 3 months both as a solution and a film on an ITO surface.

Growth of Ag Petals on Au/OA NWs and the Formation of Au/Ag MFs. Ag overgrowth onto the Au/OA NWs was achieved by introducing 2 mL of $AgNO_3$ (10 mM) and 500 μL of ascorbic acid (100 mM) into a solution containing 5 mL of as prepared Au/OA NWs. The solution was kept for 10 h for complete conversion of Au NWs into Ag flowers. The solution was centrifuged at 4000 rpm, and the residue was collected. The Au/Ag MFs formed in the intermediate stages of the reaction were collected by stopping the reaction at various time intervals. The resultant intermediate solutions were centrifuged, and the residue was washed with water and characterized.

Growth of Pt on Au/OA NWs and the Formation of Au/Pt Buds. A total of 2.5 mL of as prepared Au/OA NWs was treated with 1 mL of H_2PtCl_6 (10 mM) and 250 μL of ascorbic acid. In the case of Pt overgrowth, after 6 h of the reaction, the Au/OA NWs were completely reacted and degraded into spherical beads of Au/Pt. The Au/Pt buds formed at the intermediate stage were separated by stopping the reaction after 3 h. The material was separated by centrifugation at 4000 rpm and washed with water in order to remove the unwanted materials.

Instrumentation. Scanning electron microscopy (SEM) images and energy dispersive analysis of X-ray (EDAX) studies were done with a FEI QUANTA-200 scanning electron microscope. For SEM measurements, samples were drop-casted on an indium tin oxide (ITO) coated conducting glass and dried. Transmission electron microscopy (TEM) was carried out using a JEOL 3011, 300 kV instrument with a UHR polepiece. The samples for TEM were prepared by dropping the dispersion on amorphous carbon films supported on a copper grid and dried in ambience. UV−visible spectra were measured using a Perkin-Elmer Lambda 25 spectrometer. The mass spectrometric studies were conducted using a Voyager DE PRO Biospectrometry Workstation (Applied Biosystems) matrix assisted laser desorption ionization time-of-flight (MALDI-TOF) mass spectrometer. A pulsed nitrogen laser of 337 nm was used (maximum firing rate, 20 Hz; maximum pulse energy, 300 μJ) for the laser desorption ionization mass spectrometry (LDI MS) studies. Raman imaging of the MFs was done with a WiTec GmbH, Alpha-SNOM CRM 200 instrument having a 532 nm laser as the excitation source. The material was carefully transferred onto a cover glass, dried in ambience, and mounted on the sample stage of the Raman spectrometer. The backscattered light was collected by a 100× objective at an integration time of 50 ms. A supernotch filter placed in the path of the signal effectively cuts off the excitation radiation. The signal was then dispersed using a 600 grooves/mm grating, and the dispersed light was collected by a Peltier cooled charge coupled device (CCD).

Results and Discussion

The key factor which determines the formation of bimetallic MFs is the unusual morphology of the precursor Au/OA NWs. The precursor NW composite was synthesized (see the Experimental Section) and was well-characterized in order to derive structural information and chemical composition. The Au/OA NWs were settled as a black precipitate at the bottom of the RB flask. From the large area SEM image (Figure 1A), it is clear that this synthesis yields NWs in high yield. The yield estimated in terms of the gold content was 80−90%. From the SEM image of a single NW (Figure 1B), it is clear that they are 3−4 μm long wires with ~100 nm width. These NWs are formed by the clustering of smaller cilia-like wires of gold, which are embedded in the oligoaniline matrix. The chemical composition of these NWs was similar as in the case of Au/OA spherical nanoparticles, which was the subject of the previous investigation.[22] From the TEM analysis (Figure 1C), it was found that these NWs have a spherical tip where the number of cilia-like wires was greater, compared to the stem of the NW. Careful examination of the stem revealed the presence of an oligoaniline coating along the periphery (marked by arrows in Figure 1D) of the NW. There was no such thick coating observed at the tip of the NW. This is clear from the magnified TEM image of the tip of the NW (Figure 1E). We could also see some of the Au/OA NWs with exposed cilia-like wires at both ends. A lattice resolved image taken from the tip of the cilia-like wire is shown in Figure 1F. The d spacing of 2.35 Å corresponding to the (111) plane of Au is marked in Figure 1F. Further observations revealed that the seed NWs are multiply twinned and the lattice planes are indicated by lines in Figure 1F.

(22) Sajanlal, P. R.; Sreeprasad, T. S.; Nair, A. S.; Pradeep, T. *Langmuir* **2008**, *24*, 4607.

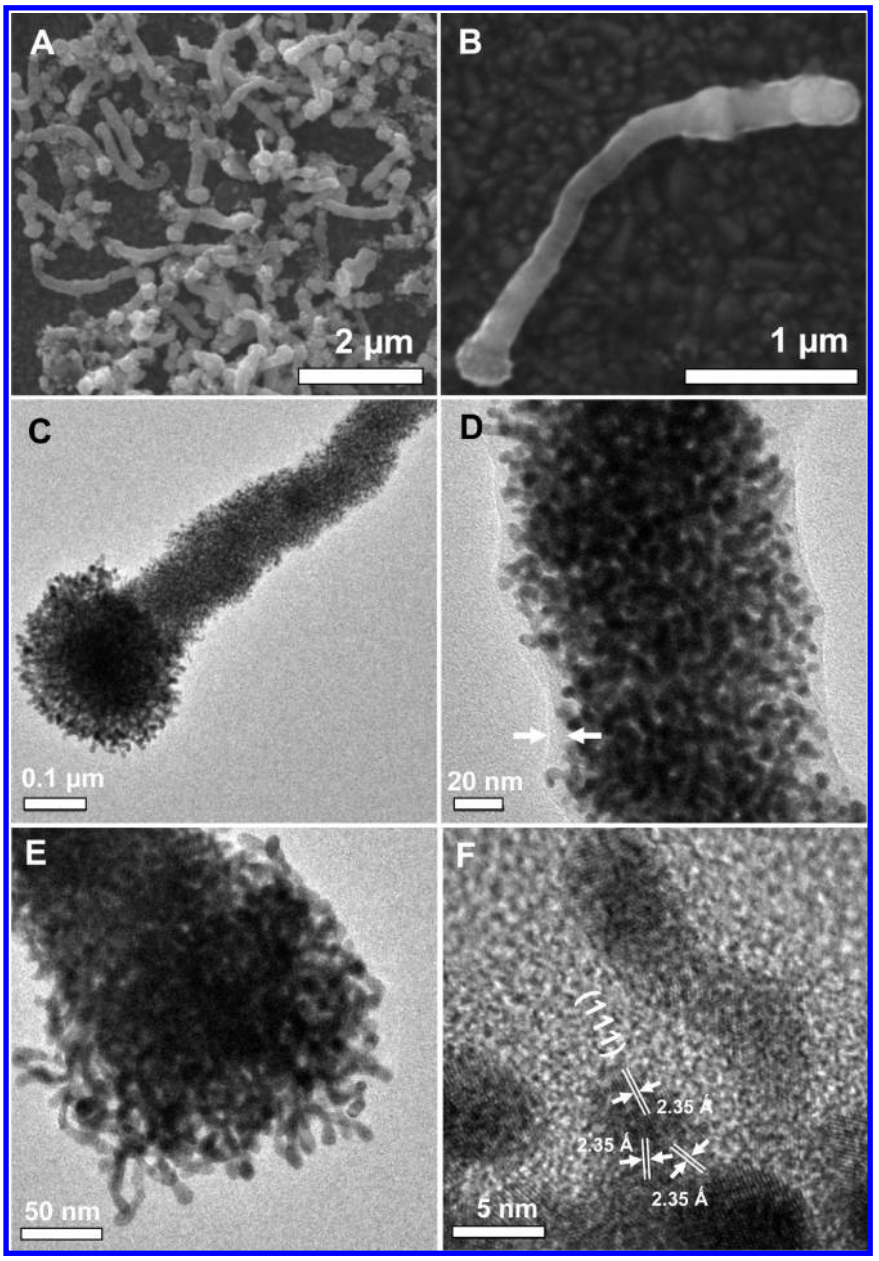

Figure 1. (A) Large area SEM image of the Au/OA NWs. (B) SEM image of a single Au/OA NW. (C−F) TEM images of various parts of the Au/OA NW in different magnifications. (C) Single NW showing a stem and tip. (D,E) Magnified views of the (D) stem and (E) tip of the NW. (F) Lattice resolved image taken from the tip of the cilia-like wires present inside the Au/OA NWs. Multiple twinning is seen in the particles shown in (F). (D) shows an oligoaniline coating on the stem (marked with arrows).

The presence of oligoaniline in the NWs was confirmed from the laser desorption ionization (LDI) mass spectrum collected from the sample. The Au/OA NWs showed two series of peaks separated with m/z 91 (see Supporting Information Figure S1), indicating the presence of oligoaniline. This separation corresponds to $-C_6H_4-NH-$. The separation between the two series of peaks (m/z 15) was due to the loss of terminal amine, $-NH$.[22] This periodic fragmentation peak clearly indicates the presence of oligomers up to the hexamer in the NWs. We have calculated the distribution of oligomers from the LDI MS data. It was found that about 45% of the oligoaniline is in trimeric form, which was the prominent peak in the LDI MS. The amounts of higher fragments such as pentamers and hexamers were very low and were ~5 and ~3.5%, respectively.

The overgrowth of Ag on the NWs is accomplished by the reduction of Ag^+ on the surface of the NWs in presence of ascorbic acid. This has resulted in the formation of flower-like mesostructures of silver with a large number of Ag petals. Just after the addition of ascorbic acid into the (Au/OA NWs)/Ag^+ mixture, Ag overgrowth was initiated at the tips and certain exposed nucleation sites of the NWs. After 10 h of the reaction, all the Au/OA NWs were completely consumed and only Ag MFs were seen in the scanning electron microscope. Almost 99% of the NWs have undergone overgrowth and converted completely into Ag MFs. The large area SEM image of the MFs formed after 10 h of the reaction is shown in Figure 2. This particular morphology includes a flower with a large number of Ag petals (inset of Figure 2). About 90% of the particles had flower-like morphology, and the rest of the nanoparticles were assorted and spherical in shape. A TEM image of a single Ag mesostructure formed after 10 h of the Ag overgrowth is shown in Figure 3. The d spacing of 2.35 Å shown in the lattice resolved image (inset of Figure 3), taken

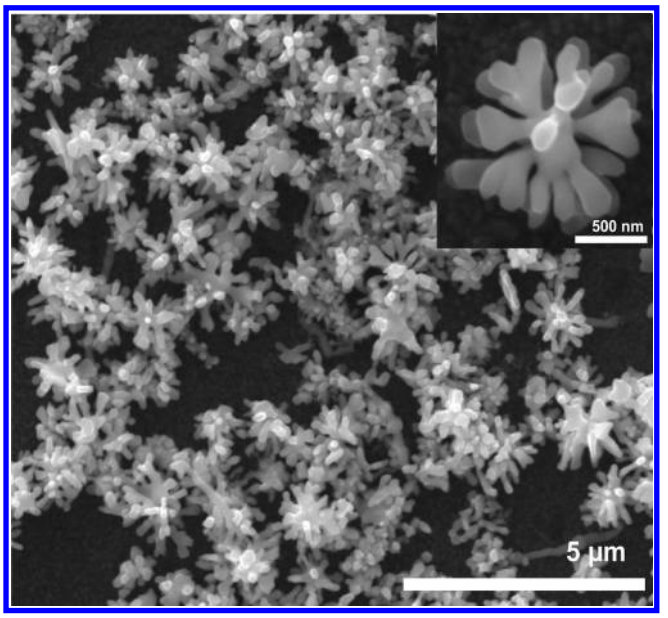

Figure 2. Large area SEM image of the Ag MFs formed after 10 h of growth. Inset shows the enlarged view of a single Ag MF.

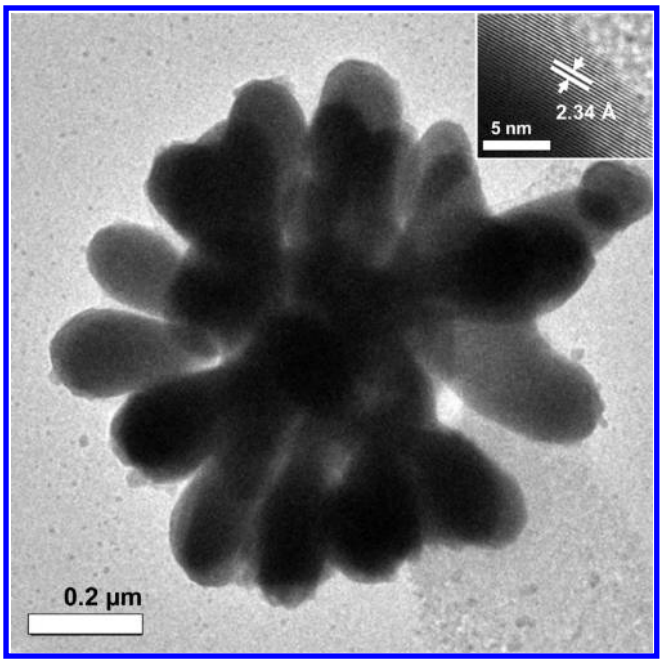

Figure 3. TEM image of a single Ag MF and its lattice resolved image (inset).

from the tip of a single Ag mesoflower detached from the Au/OA NW after complete growth, corresponds to the (111) plane of Ag.

The sequential conversion of the Au/OA NWs into various shapes including Ag MFs and Au/Ag MFs may be represented as shown in Scheme 1. The silver ions added are reduced by ascorbic acid at certain regions on the surfaces of Au/OA NWs. Since the Au particles at the tip of the NW are more exposed compared to the body, the reaction happens mostly at the tip. This leads to the formation of a bimetallic MF of Ag with a Au stem. Experiments suggest that the conversion of the NWs to Ag MFs happens in stages. The first stage of silver overgrowth on each NW is over almost completely by 3 h of the reaction. Figure 4 shows the large area SEM image of the Au/Ag bimetallic MFs separated after 3 h. The SEM image of the

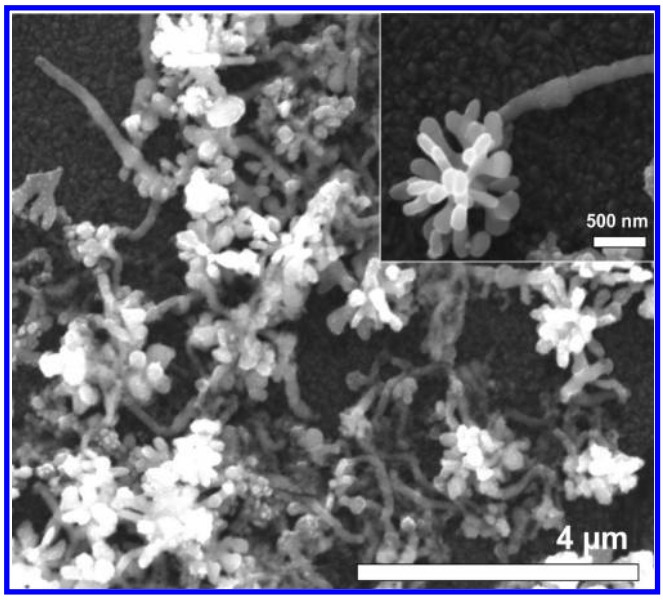

Figure 4. Large area SEM image of the Au/Ag bimetallic MFs separated after 3 h of the reaction. Inset shows a single bimetallic Au/Ag MF.

Scheme 1. Schematic of Various Stages of the Formation of a Au/Ag MF

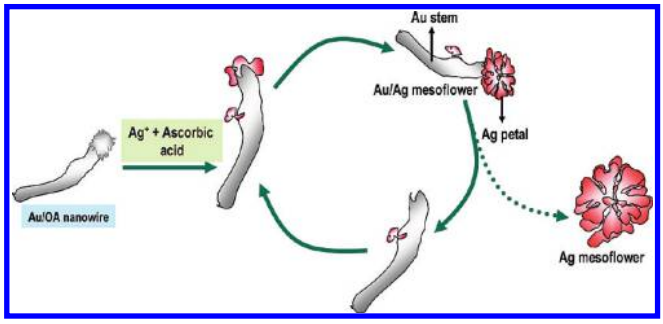

single bimetallic mesoflower (inset of Figure 4) reveals the unusual 3D growth of Ag onto the Au/OA NWs, forming a Au/Ag MF. TEM images of the Au/Ag MFs separated after 30 min and 3 h are shown in Supporting Information Figure S2. Blossoming of the Ag flower at the tip of the Au/OA NW was clear from the TEM images. After the completion of overgrowth, the Ag flower detached from the Au/OA NW. The remaining part of the NW again acted as a nucleation site for further growth of the Ag MF. This process continued until the NW was completely consumed.

The chemical composition of the bimetallic MF was analyzed by EDAX. SEM images and corresponding elemental maps of the systematic evolution of the mesostructures have been captured (Figure 5). An SEM image and the corresponding EDAX image of a Au/OA NW are presented in Figure 5A and B. The EDAX image shows the uniform distribution of Au along the NW (Figure 5B). A small increase in the Au content toward the tip may be due to the slightly larger dimension there. Figure 5C and D (SEM and EDAX images of a Au/Ag bimetallic mesoflower separated after 3 h) reveals that the stem of this mesomaterial is composed of gold and the petals nucleated at the tip of the NW are made of silver. Since the overgrowth happened only at the tip, there was no Ag content present at the stem after 3 h. These Ag flowers are composed of a large number of petal-like silver nanoplates, and are nucleated from the tips of Au/OA NWs, resulting in bimetallic MFs. The thickness of these petals was in

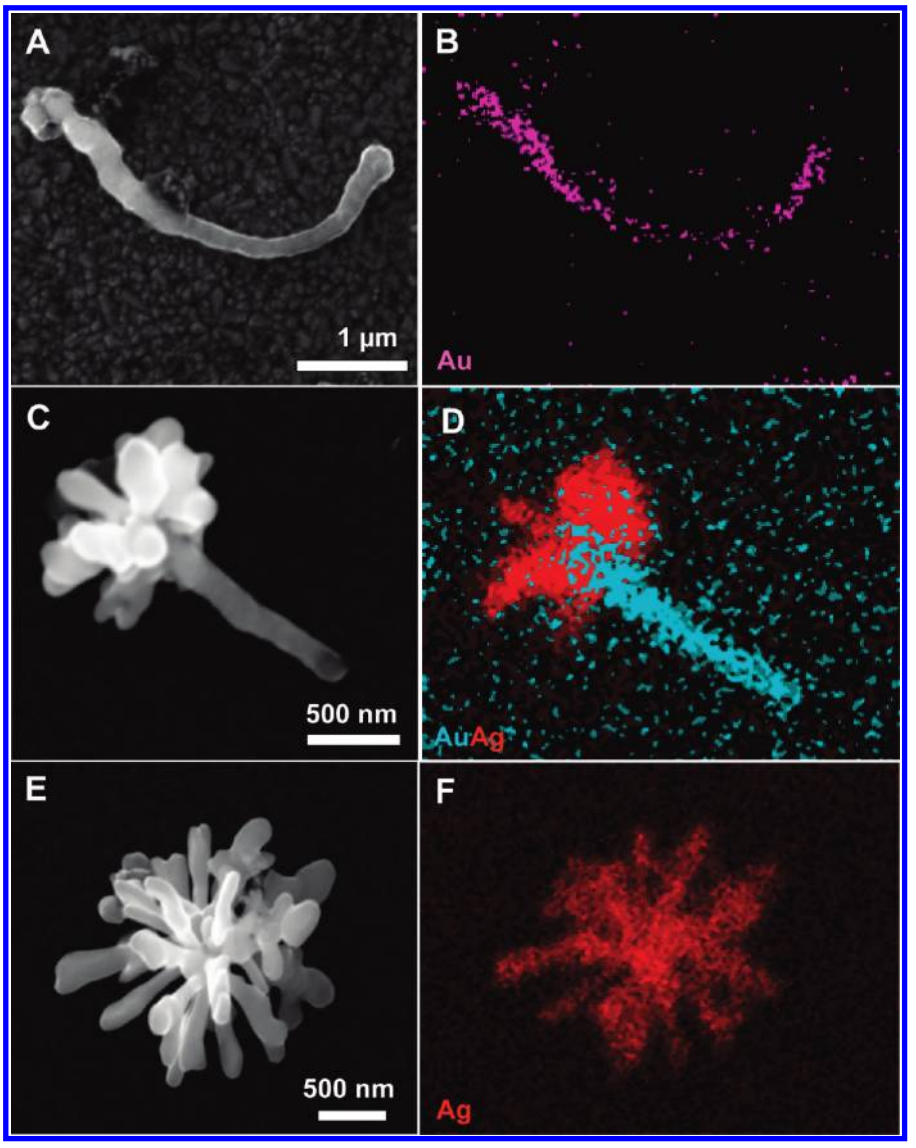

Figure 5. SEM and respective EDAX images of the Au/OA NW and different mesostructured materials formed at various stages of the Ag overgrowth. (A,B) Au/OA NW, (C,D) after 3 h, and (E,F) after 10 h.

the range of 75−100 nm. The petals originate from a central core and are grown in all directions, forming 3D MFs of Ag. The elemental analysis of a Ag MF, detached from a Au/OA NW, shows the presence of Au in it (see Supporting Information Figure S3). This confirms that the end of the Au NW acting as the nucleation site for the Ag overgrowth, remains inside the MF even after the detachment. This explains the complete consumption of Au NWs in the growth process. SEM and EDAX images of the Ag MF separated after 10 h are shown in Figure 5E and F, respectively.

We could also isolate mesostructures of another kind, which have Ag flowers on both ends of the Au stalk, along with the Au/Ag MFs formed after 3 h. This is likely to happen as a result of Ag overgrowth of Au/OA NWs with exposed nucleation sites at both ends of the NW. The number of such flowers was very few. SEM and corresponding EDAX images of the Au/Ag flowers at both ends of the Au/OA NW is shown in Figure 6.

To further demonstrate the controllability of our present method, we extended the same approach to make bimetallic mesoparticles of Au and Pt. Interestingly, we observed the overgrowth of Pt onto the Au/OA NWs to form Au/Pt buds instead of flowers. We studied the overgrowth of Pt on the Au NWs by monitoring the reaction at various time intervals. Figure 7A shows the large area SEM image of Au/Pt mesobuds formed after 3 h of the reaction of Au/OA NWs with chloroplatinic acid and ascorbic acid. Pt can grow epitaxially onto the gold nanoparticle surface.[23] In contrast with the silver overgrowth, occurring at the tip of the NW, platinum showed an overgrowth throughout the stem besides the tip. After continuing the reaction for 6 h, as in the case of the Ag overgrowth, the Au/OA NWs almost completely degraded and converted into spherical Au/Pt beads (Figure 7B). The Pt overgrowth on the Au NWs is confirmed from the elemental map of the mesostructures separated after 3 h (Figure 7C−E) and 6 h (Figure 7F−H). EDAX images show the presence of Pt and Au. Even though the extent of overgrowth at the tip was high, Pt deposition was also visible throughout the entire stem of the Au/OA NWs. The EDAX spectrum (see Supporting Information Figure S4) confirms the composition of the mesoparticles. Figure 8 shows TEM images of the Au/Pt mesobud (Figure 8A) and Au/Pt bead (Figure 8B). It is clear from the TEM images that Pt gets coated on the Au/OA NW

(23) Shiigi, H.; Yamamoto, Y.; Yoshi, N.; Nakaob, H.; Nagaoka, T. *Chem. Commun.* **2006**, 4288.

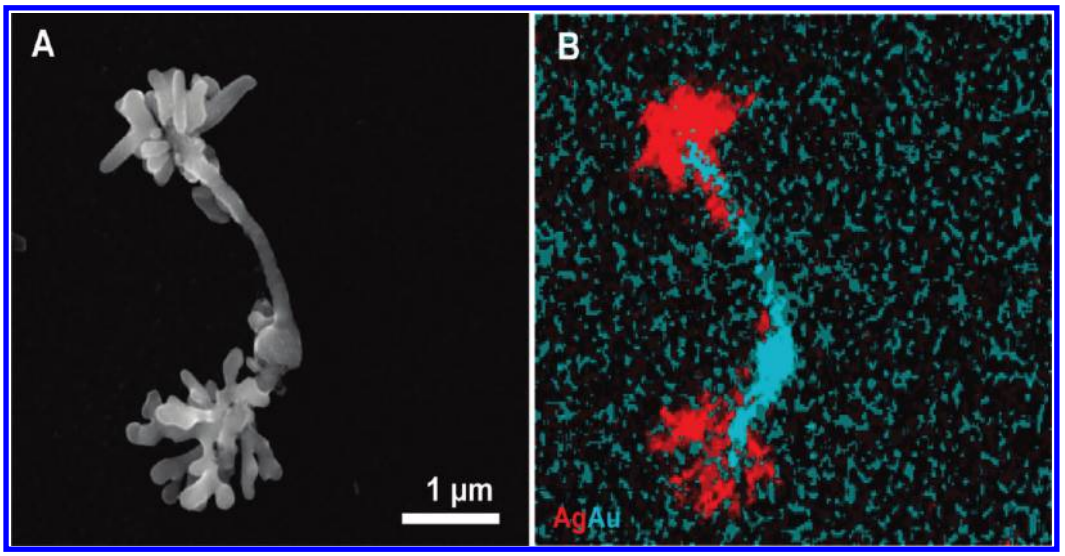

Figure 6. (A) SEM and corresponding (B) EDAX images of the mesostructures with Ag flowers on both ends of the Au stalk formed after 3 h.

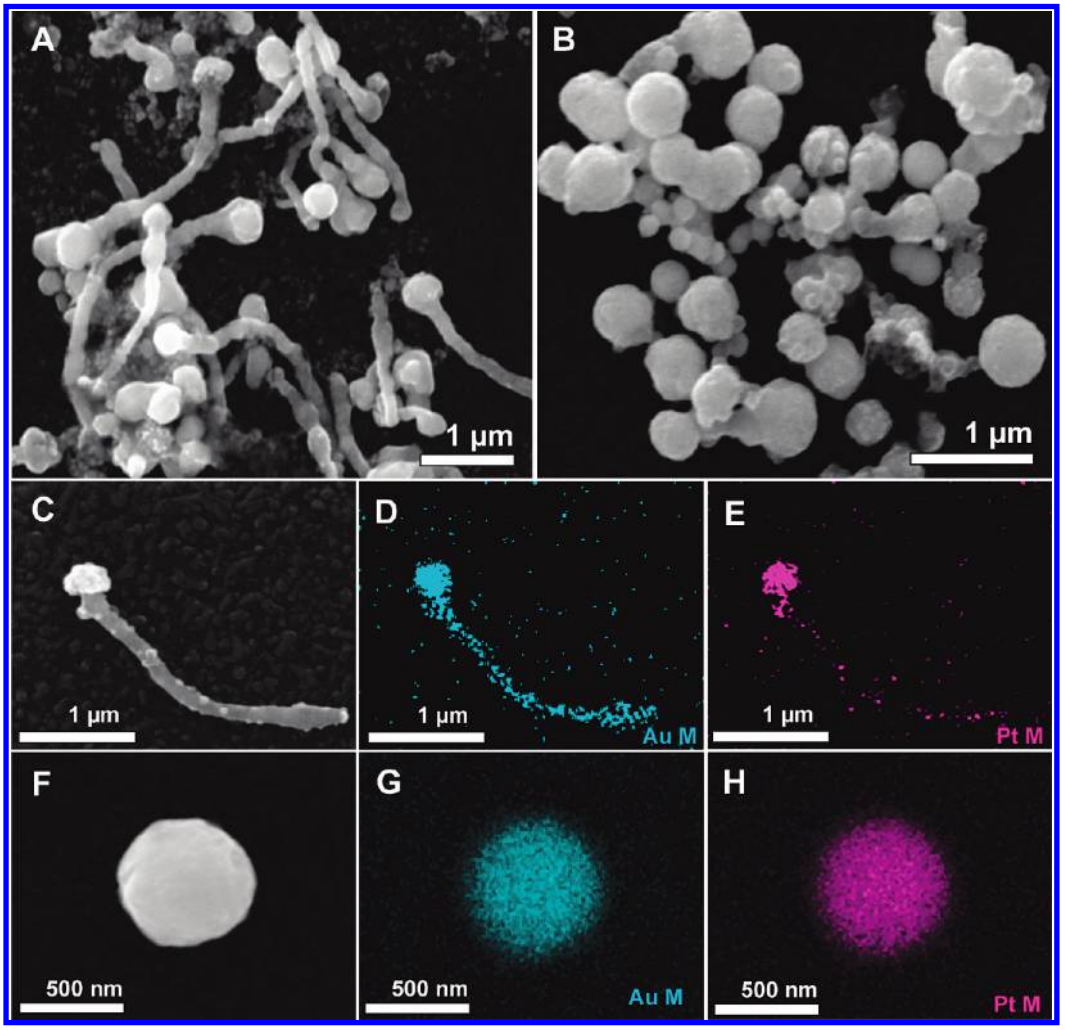

Figure 7. Large area SEM images of the (A) Au/Pt mesobuds and (B) Au/Pt beads formed after 3 and 6 h. (C−H) SEM and corresponding EDAX images at different time intervals of Pt overgrowth reaction on Au/OA NWs. (C) is the SEM image of a Au/Pt mesobud formed after 3 h. (D) and (E) correspond to EDAX images of (C). (F) is a Au/Pt bead detached from the Au NW after 6 h. (G) and (H) are the EDAX images of (F) based on Au Mα and Pt Mα.

in a dendritic fashion and appears as smaller hairs at the surface of the beads. A lattice resolved image taken from these hairs is shown in Figure 8C.

These hairs showed a *d* spacing of 2.25 Å, which corresponds to the (111) plane of platinum. It is clear from the high resolution image that there is no polymeric cover on the Pt overgrowth,

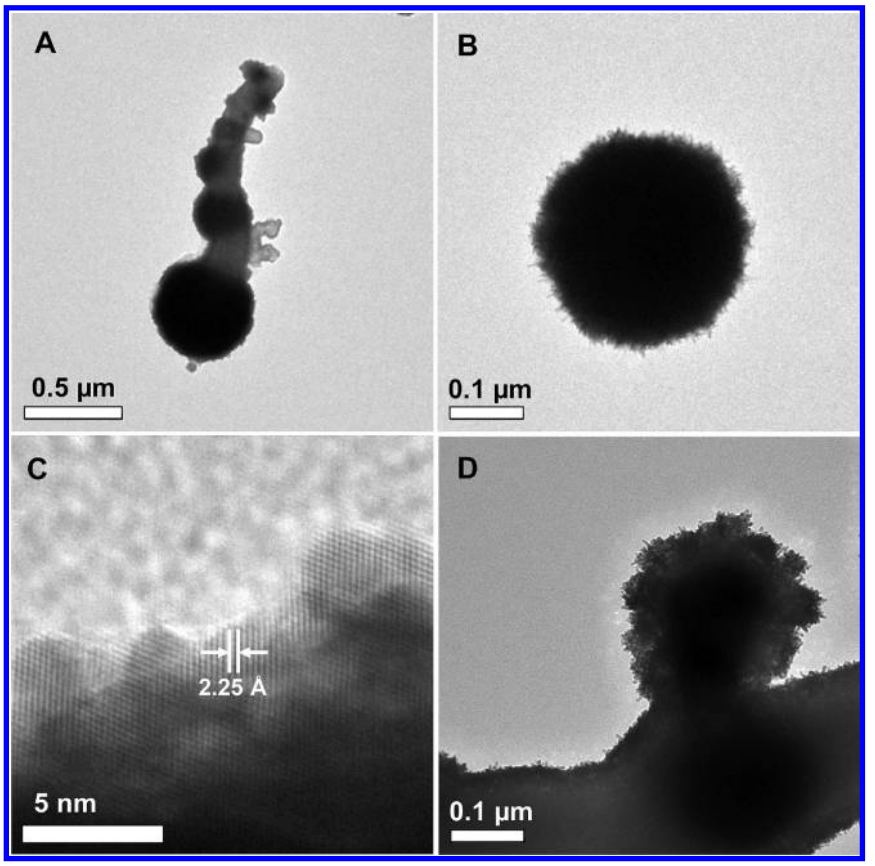

Figure 8. TEM images of a (A) Au/Pt mesobud and (B) Au/Pt bead, separated after 3 and 6 h, respectively. (C) Lattice resolved image taken from the tip of the dendritic hairs of the Au/Pt bead. (D) Pt overgrowth at the stem of the Au/OA NW.

unlike in the case of AuNWs. Figure 8D reveals the Pt overgrowth on the stem of the Au/OA NW.

We studied the growth and evolution of the MFs using optical absorption measurements. UV−vis spectra collected at different stages of Ag overgrowth on Au/OA NWs are shown in Figure 9A. Trace 1 represents the absorption spectrum of the precursor Au/OA NWs. The broad peak observed at 560 nm could be attributed to a combination of the excitonic-type transition in the quinoid unit of the oxidized aniline and the surface plasmon of the gold.[22,24] The broad absorption peaks observed around 440 and 740 nm are the respective localized and delocalized polaron bands of the oligoaniline coating present on the NW surface.[21−25] As the overgrowth progresses, the absorption due to the oligoaniline was masked by the SPR of the Ag particles formed in the solution. The peak at 560 nm showed a blue shift and finally disappeared after 10 h. This confirms the degradation of the Au/OA NWs into smaller wires during the overgrowth. After the addition of Ag^+ and ascorbic acid, a new peak emerged around 420 nm, which is clear in the absorption spectrum taken after 30 min of the reaction. This new absorption peak pointed toward the overgrowth of Ag on Au NWs, and it is attributed to the SPR of Ag MFs formed at the tip of the Au NWs. As the reaction proceeded, the intensity ratio between the SPR situated around 420 and 560 nm started increasing, which indicates the degradation of Au NWs and simultaneous growth of the Ag MFs. After 10 h of the reaction, the absorption centered around 560 nm disappeared completely and only an absorption due to the Ag MFs was observed. This suggests the complete degradation of the Au/OA NWs. It was noted that, as the reaction progressed, the SPR centered around 560 nm was slightly blue-shifted whereas the peak around 420 nm was red-shifted. This observed shift in the absorption maxima confirmed the gradual degradation of Au/OA NWs and simultaneous growth of Ag MFs.

The Pt overgrowth on the Au/OA NWs was monitored using UV−vis spectroscopy. The overcoating of Pt resulted in the disappearance of the SPR of Au/OA NWs centered around 560 nm and showed a wider absorption in the visible range (Figure 9B). It is known that the coating of one metal on the other in a core−shell-like nanostructure results in the damping of the SPR of the core.[26] This may be attributed to the change in the dielectric environment around gold as well as the large scattering by the dendritic Pt shell.[27] Though the possibility of the alloy formation cannot be ruled out at the interface, elemental maps and high resolution TEM studies suggest the absence of alloy formation at the surfaces of Au/Pt beads. Thus, by introducing bimetallicity into the Au NWs, we demonstrate tuning of the optical property of the nanoparticles.

The site specific overgrowth of various metal ions is attributed to the unusual morphology of Au/OA NWs. The extent of oligoaniline coating at the tip was comparatively less than that at the stem. This creates more exposed cilia-like wires at the tip of the NW. These exposed areas can act as the nucleation sites for the overgrowth of various metals. Since there is a close similarity in

(24) Nekrasov, A. A.; Ivanov, V. F.; Vannikov, A. V. *J. Electroanal. Chem.* **2000**, *482*, 11.
(25) Xiang, Y.; Wu, X.; Liu, D.; Li, Z.; Chu, W.; Feng, L.; Zhang, K.; Zhou, W.; Xie, S. *Langmuir* **2008**, *24*, 3465.
(26) (a) Mulvaney, P.; Giersig, M.; Henglein, A. *J. Phys. Chem.* **1992**, *96*, 10419. (b) Mulvaney, P. *Langmuir* **1996**, *12*, 788. (c) Garcia-Gutierrez, D. I.; Gutierrez-Wing, C. E.; Giovanetti, L.; Ramallo-Lopez, J. M.; Requejo, F. G.; Yacaman, M. J. *J. Phys. Chem. B* **2005**, *109*, 3813.
(27) Guo, S.; Wang, L.; Dong, S.; Wang, E. *J. Phys. Chem. C* **2008**, *112*, 13510.

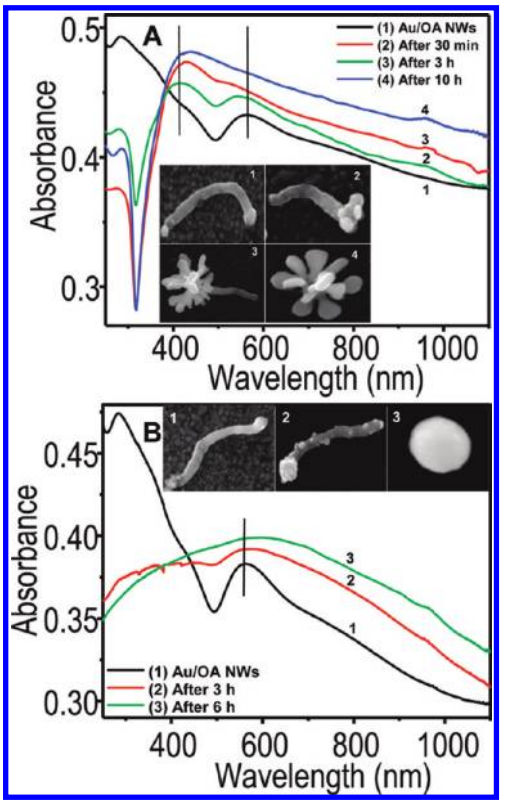

Figure 9. UV−vis spectra of (A) Ag and (B) Pt overgrowth on Au/OA NWs taken at various time intervals. Traces 1−4 in panel (A) are the spectra collected at 0, 0.5, 3, and 10 h, respectively, of Ag overgrowth. Traces 1−3 in panel (B) show the spectra collected at 0, 3, and 6 h, respectively, of Pt overgrowth. Representative SEM images of single particles collected at respective stages of the reaction are shown along with the spectra.

crystal structures and lattice parameters between gold and silver, the silver atoms can preferentially nucleate and grow epitaxially[2a,21] at the nucleation sites present on these cilia-like wires. Because of the presence of large number of nucleation sites at the tip, the reactivity of the NW will be high at the tip. This results in the specific overgrowth at the tip compared to the stem of the NW. It is also possible to have nucleation sites at the stem of the NW. This may happen largely by the loose binding of the oligoaniline coating at the stem or by the rupturing of oligoaniline. The growth is evident from the SEM images.

Although the mechanism of breakage of the MFs is not completely clear, we propose the following tentative argument. As we can see from the lattice resolved TEM image, the cilia-like structures of Au/OA NWs are multiply twinned in nature. Randomly oriented (111) planes in a single seed particle are clearly seen in the lattice resolved TEM image. The reduction and the subsequent growth of the silver petals at the Au/OA NW surface happen by epitaxial growth from these multiply twinned nucleation sites. This results in the formation of randomly oriented Ag petals. The formation of bigger flowers at the tip will perturb the center of mass of the whole NW, which will shift more toward the tip as the growth happens. Consequently, the strain generated inside the stem of the NW will lead to the breakage of the NW at the very end of the tip. After 3 h of the reaction, the Ag overgrowth reaches its maximum limit, and further reaction leads to the rupturing of the NW at the end of the tip where the overgrowth occurred. Oligoaniline is present at the Au/Ag interface which may facilitate the breakage. In fact, the latter may be the better reason for the breakage as the length of the Au NW decreases with an increase in reaction time. We could see several isolated Au/OA NWs with reduced length at different areas of the ITO plate after 6 h of the reaction (see Supporting Information Figure S5). Compared to parent NWs (3−4 μm), these degraded NWs had a reduced length in the range of 0.5−1 μm. Ag overgrowth was evident at the surface of the individual broken NWs (see Supporting Information Figure S5). This suggests the degradation of the Au NWs and the gradual formation of Ag MFs. The detachment of the MFs will create a greater number of exposed nucleation sites at the newly formed tips of the Au/OA NWs. The excess Ag ions present in the system again start getting reduced at these exposed areas of the Au/OA NWs. This will continue until the NW and the Ag ions are fully consumed. After 10 h of the reaction, we found that the Au NWs are fully reacted and converted into Ag flowers. Only very few Au/OA NWs were seen after the complete growth. This validates the sequential degradation of Au/OA NWs during the growth of silver MFs. In the case of Pt overgrowth, the addition of chloroplatinic acid into the Au/OA NWs reduces the pH of the medium, and subsequent rupturing of the oligoaniline coating over AuNW occurs. This creates a greater number of nucleation sites throughout the entire body of the Au/OA NWs, and subsequent overgrowth happens at these exposed sites. This may result in the pronounced overgrowth at the stem in the case of Pt compared to Ag. This was confirmed from the EDAX image of the Au/Pt mesobuds.

We investigated the morphology and chemical structure of the Au/Ag MFs using Raman spectroscopy and microscopy. The presence of oligoaniline coating on the surface of these bimetallic MFs was exploited for the SERS study. The electromagnetic enhancement mechanism of SERS involves the enhancement of the Raman scattering cross section of the analyte molecule, when they are present within the electric field of the metal nanoparticles, produced by the excitation of surface plasmons. Enhancement factors of the order of 10^9 have been seen in anisotropic nanostructures.[21c,30] We expect significant enhancement of the Raman bands of oligoaniline molecules coated on metal surfaces of the MFs when they are irradiated by 532 nm. Variation in the SERS intensity is also expected from different metal domains, silver, gold, and platinum.

As oligoaniline is highly Raman active, we took this advantage to image the bimetallic MFs using their Raman features. A Raman based image of a single mesoflower and its 3D view based on the integrated spectral intensities ranging from 300 to 2000 cm^{-1} are shown in Figure 10A and B, respectively. The optical image of the bimetallic MF selected for the Raman study is shown in the inset of Figure 10A. A considerable enhancement in the intensities of the Raman features occurs where oligoaniline is adsorbed on silver (Figure 10E). The spectral features are the same in both of the regions (Figure 10E), but the intensities are different. This is attributed to the extent by which the features are enhanced. It is unlikely to be due to any difference in the quantity of OA present in these regions. If at all such changes are possible, OA is expected to be more in Au rich regions than in Ag rich regions as the parent Au NWs were made with OA. The enhancement in the Ag region can also be attributed to the larger possibility of hot spots in the region, in comparison to the stem.

The Raman bands of oligoaniline at 1615 cm^{-1} (C−C stretching), 1560 cm^{-1} (C=C stretching), 1486 cm^{-1} (C=N stretching), 1105 cm^{-1} (C−H bending), 992 cm^{-1} (ring deformation), and 847 cm^{-1} (ring deformation) are well-known.[28] It was also noted that certain vibrations, collected from the Au stem, were feeble (Figure 10E). The 992 cm^{-1} band, assigned to ring

(28) Choi, C. H.; Kertesz, M. *Macromolecules* **1997**, *30*, 620.

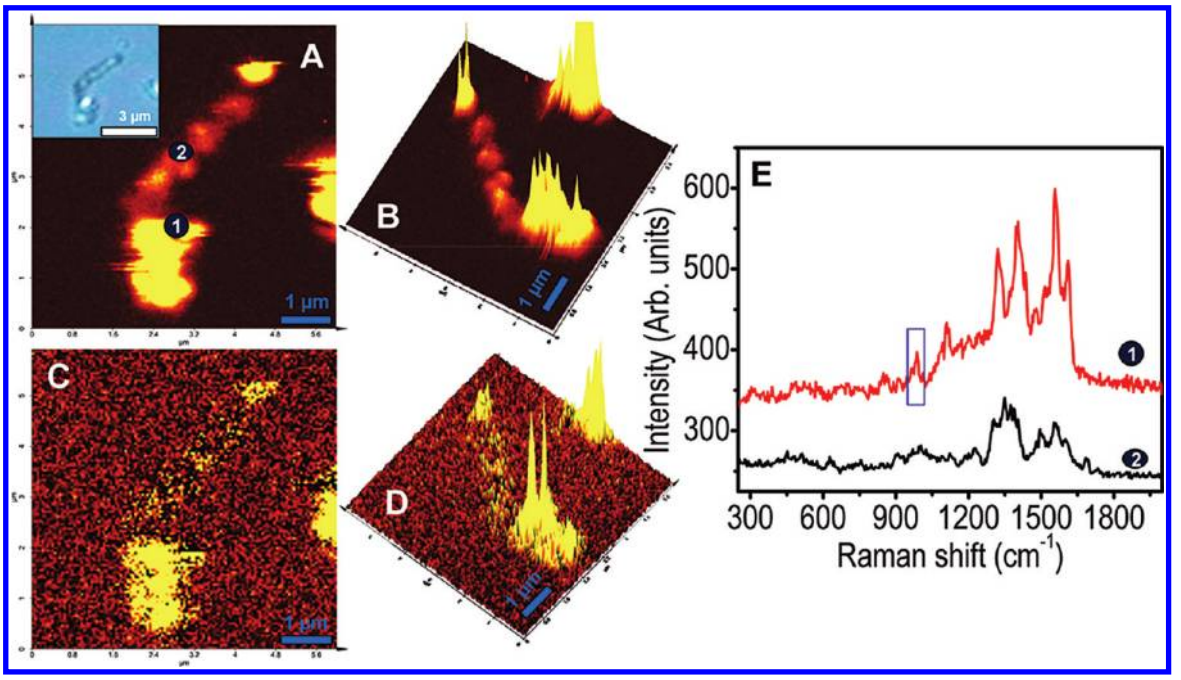

Figure 10. (A−D) Raman images and the corresponding 3D views of a single bimetallic Au-stalked Ag mesoflower synthesized after 3 h of the reaction. Inset of (A) is the white light optical image of the meso/nanostructure used for Raman imaging. The Raman image is created by integrating Raman spectral intensities between 300 and 2000 cm^{-1} collected from an area of 6 μm × 6 μm. (E) Raman spectra collected from different locations of the Au-stalked Ag flower marked in (A). (C) and (D) are the Raman spectral images of the same Au-stalked Ag flower, by integrating the SERS intensities between 925 and 1025 cm^{-1} marked in (E).

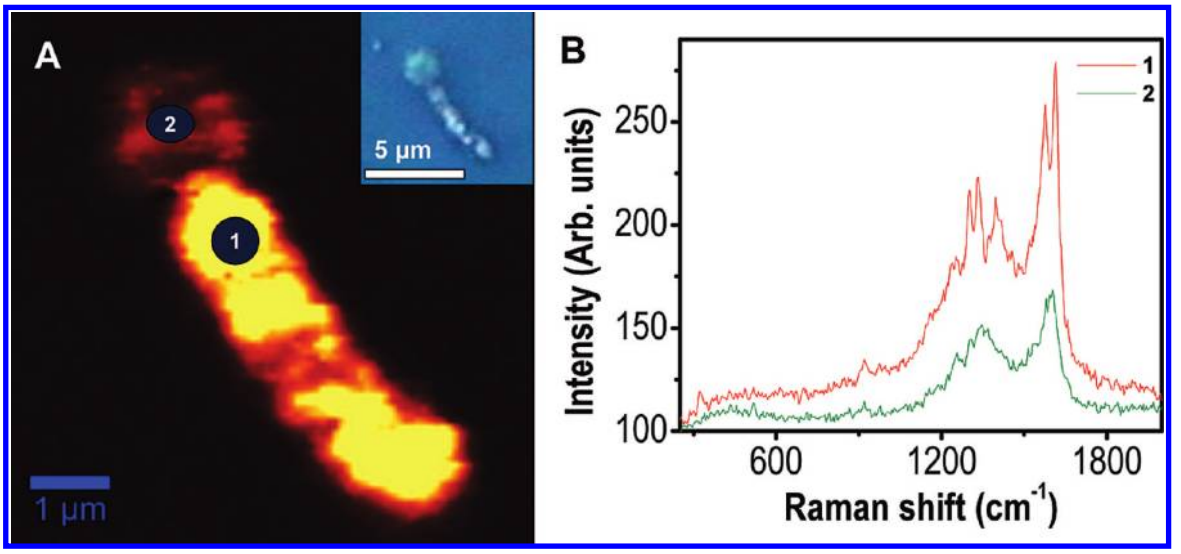

Figure 11. (A) Raman image of a single bimetallic Au/Pt mesobud synthesized after 3 h of the reaction. Inset of (A) is the white light optical image of the Au/Pt mesobud used for Raman imaging. The Raman image was created by integrating Raman spectral intensities between 300 and 2000 cm^{-1}. (B) Raman spectra collected from different locations of the Au/Pt mesobud marked in (A).

breathing mode of the terminal rings, is often called the trigonal ring breathing.[29] This was very weak in the case of oligoaniline adsorbed on the Au stem compared to the Ag flower. This deformation mode is useful for the characterization of inner and outer aromatic rings of the oligoaniline molecule. The ring breathing mode also gives an idea about the number of aromatic rings in the oligomer, and it gets weaker as the number of rings increases.[29] A Raman spectral image and corresponding 3D view of the Au/Ag MF derived from the SERS intensity of the ring deformation between 925 and 1025 cm^{-1} are shown in Figure 10C and D. The SERS intensity of the ring deformation was strong on the Ag flower, but it was weak on the Au stem. This may be due to the close packing of the oligoaniline molecule on the Au stem, which restricts the ring deformation to some extent, hence its weakness. An additional reason could be the closeness of the plasmon resonance of the Ag MF to the excitation wavelength.

In order to check the substrate dependent SERS activity, Raman images of Au/Pt mesobud were also collected. Figure 11A shows the Raman image of a single bimetallic Au/Pt mesobud created by integrating the spectral intensities ranging from 300 to 2000 cm^{-1}.

(29) Boyer, M.-I.; Quillard, S.; Rebourt, E.; Louarn, G.; Buisson, J. P.; Monkman, A.; Lefrant, S. *J. Phys. Chem. B* **1998**, *102*, 7382.
(30) Sajanlal, P. R.; Pradeep, T. *J. Nanosci. Nanotechnol.* **2009**, *9*, 5283–5287.

From the Raman spectra (Figure 11B), it was found that the SERS activity varies at different locations of the Au/Pt mesobud. In contrary to the case of the Au/Ag MFs, the SERS intensity was low at the tip compared to the stem of the Au/Pt mesobud. This is pointing toward the low SERS activity of Pt compared to Au. In the case of Au/Pt mesobuds, the tip is covered by Pt and the stem is mainly composed of Au. The reduced SERS intensity of the Au/Pt mesobud may be due to the difference in the Raman excitation wavelength and surface plasmon of the Pt.

Conclusions

In conclusion, we showed that specially made NWs of gold (Au/OA NWs) can be manipulated to complex hybrid architectures by a simple overgrowth reaction. The overgrowth could be controlled in order to make bimetallic Au/Ag MFs and Au/Pt mesobuds. The incorporation of Ag and Pt onto Au wire and subsequent shape transformation is an example of the successful tuning of the optical property of nanoparticles by introducing two different metals. Raman based spectral imaging of the bimetallic MF reveals the molecular details and the nature of interaction of oligoaniline to different metal domains in the mesostructures. Raman study also suggests a substrate effect due to Ag and Au on the SERS property. It appears that the process of overgrowth of Ag and Pt is controlled by the structure of the NWs. Although the mechanism of growth of the MFs and their subsequent termination are uncertain, it is clear that the twinned particles in the embedded OA matrix allow the overgrowth to occur in certain directions. A similar approach can be used to make hybrid nanomaterials of different metals of desired composition, which would find applications in sensing and surface-enhanced Raman spectroscopy, in particular.

Acknowledgment. We thank the Department of Science and Technology, Government of India for constantly supporting our research program on nanomaterials.

Supporting Information Available: LDI MS of Au/OA NWs, TEM images of the intermediate bimetallic Au/Ag MFs, EDAX spectrum of Ag MF and Au/Pt bead, and SEM images of the intermediate Au/Ag mesostructures formed. This material is available free of charge via the Internet at http://pubs.acs.org.